

Any DOF all at once: single photon state tomography in a single measurement setup

Roey Shafran^{1,†}, Ron Ziv^{1,†}, Mordechai Segev^{1,2,*}

¹Department of Electrical and Computer Engineering, Technion – Israel Institute of Technology, Haifa 32000, Israel

²Physics Department, Technion – Israel Institute of Technology, Haifa 32000, Israel

[†]These authors contributed equally to this work

^{*}msegev@technion.ac.il

Abstract

Photonic quantum technologies utilize various degrees of freedom (DOFs) of light, such as polarization, frequency, and spatial modes, to encode quantum information. In the effort of further improving channel capacity and increasing the complexity of available quantum operations, high-dimensional and hyperentangled states are now gaining interest. Efficiently measuring these high dimensional states is challenging due to the large number of measurements required for reconstructing the full density matrix via quantum state tomography (QST), and the fact that each measurement requires some modification in the experimental setup. Here, we propose a framework for reconstructing the density matrix of a single-photon hyperentangled across multiple DOFs using a single intensity-measurement obtainable from traditional cameras, and discuss extensions for multiphoton hyperentangled states. Our method hinges on the spatial DOF of the photon and uses it to encode information from other DOFs. We numerically demonstrate this method for single-photon OAM-spin and OAM-frequency entangled states using an ideal coupler and a multimode fiber, to perform the spatial information mixing and encoding. This technique simplifies the experimental setup and reduces acquisition time compared to traditional QST based methods. Moreover, it allows recovery of DOFs that conventional cameras cannot detect, such as polarization, thus eliminating the need for projection measurements.

Introduction

Photonic quantum technologies have gained significant interest in recent years due to the favorable properties of photons, among them lack of decoherence, scalability and compatibility with standard technologies such as optical fibers and integrated photonic circuits [1,2]. Therefore, there is clear interest in developing photonic-based applications in many areas of

quantum technology ranging from quantum communication [3] to simulations of complex quantum systems [4] and quantum computation [5] .

At the base of quantum information technologies stands entanglement, which relies on the physical degrees of freedom (DOFs) in which quantum information (e.g., qubits) can be encoded. In photonics, commonly used DOFs include polarization and momentum, the latter offering spatial path entanglement [6,7]. Yet the complex structure of light offers many additional DOFs, all controllable, and each offering a Hilbert space suitable for quantum information encoding. Examples include frequency and time-bins (using temporal and spectral structures) [8,9], and spatial DOFs such as orbital angular momentum (OAM) [10–13]. Moreover, to further increase the information density per physical constituent of the system, it is possible to use DOFs that offer more than two levels per particle, for example OAM, and move the information coding from qubits to high dimensional qudits, or to utilize states with multiple DOFs per particle. The latter, known as hyperentangled states [14], involve entanglement across multiple DOFs, have been gaining much interest recently. The use of hyperentanglement open the door to increased performance in virtually all applications of quantum information, ranging from higher channel capacity [12,15,16] and enhanced security [17] to noise robustness [13,18] in quantum communication, and allows for more complex [8,19] and deterministic quantum operations [8,20,21].

Naturally, the use of entangled states requires means to measure them in an efficient manner and recovering the information they encode. Standard approaches for reconstructing photonic states, rely on quantum state tomography (QST) [22–25], which requires measurements of the complete set of observables accounting for all the real values of the density matrix representing the quantum state. In an experimental setup, probing different observables amounts to varying the configurations of polarizers and spatial light modulators for different spin-spatial modes [24,25], or phase shifters and interferometers [8,9] in the case of frequency/time bins, and click detectors to record coincidences in the case of multi-photon states. This, poses a problem even when considering the relatively simple case of qubits. Namely, recovering the density matrix of n qubits requires 2^{2n} measurements, which becomes exceedingly difficult for large n . Using high-dimensional DOFs and hyperentanglement instead of qubits makes this problem far more severe even for small n , as the number of required measurements scales linearly with the dimensionality of each DOF and exponentially with the number of entangled DOFs. For instance, characterizing a photons entangled in polarization and a 2-level OAM system requires 16 measurements [26]. If the OAM system is extended to 6 dimensions, the

number of measurements increases to 144. Introducing an additional DOF, such as a 4-level frequency-bin system, raises the requirement to 256 measurements. Adding more DOFs and increasing each of their dimensions leads to more measurements, making the tomography process unfeasible. Obviously, having to carry out so many different measurements in different configurations also induces noise into the system, while also increasing the calibration needs of the setup. Clearly, it is highly desirable to reduce the number of measurements required to fully characterize a quantum state, especially when it is hyperentangled.

These insights motivated a rich body of work that aims at simplifying the measurement setup and reducing the number of different quantities needed to characterize the quantum state. Several approaches achieved measurement reduction by leveraging known state structures [27], using single observable QST with ancilla modes [28,29], and exploiting spatial structure to enable tomography with minimal projections or reference interference [30,31]. All these works share in common the usage of the inherent structure of the signal, whether given or specifically engineered, to facilitate improved performance in the recovery of the quantum information. However, the recovery of a quantum state displaying entanglement between multiple DOFs using a single measurement has never been proposed.

Here, we propose a general framework for reconstructing the density matrix of a single-photon entangled across multiple DOFs using a single intensity measurement. Additionally, we provide extensions for multiphoton hyperentangled states by transitioning from intensity to coincidence measurements. Our framework leverages the spatial DOF of the photon to encode the information transferred to it from the different DOFs, and utilize the coupling between the different spatial DOFs for complete recovery of the state. We demonstrate our method numerically for single-photon qudits entangled in OAM-spin and in OAM-frequency-bin, showcasing results for both an ideal random coupler and a physical realization based on a multi-mode fiber. Necessitating only a single intensity measurement, our framework can significantly simplify experimental setups and reduce acquisition time compared to traditional click-based or projective measurement schemes. Remarkably, our method enables the recovery of DOFs for which standard imaging devices are blind to, such as polarization, exemplifying the ability to remove the need of projection measurements for quantum information borne on single photons.

Theory

Our proposed system relies on intensity measurements of the photonic state. We begin by establishing the relationship between the measured intensity at a given pixel (x, y) and the quantum measurement of that pixel, informally given as $Tr[|x, y\rangle\langle x, y|\rho]$, which will be formally defined in the following sections. Through the analysis, we highlight fail-cases and demonstrate how by using a coupler we can obtain complete state recovery.

We first introduce the concept of spatial photon modes, following the formulation in [32], as these modes dictate the distribution of photon probabilities at some plane in free space (henceforth denoted as the "imaging plane"). The modal creation and annihilation operators \hat{a}_m^\dagger and \hat{a}_m respectively create and annihilate a photon in mode m . A single-photon excitation (i.e., adding one photon to the vacuum state) in mode m is denoted by $|f_m\rangle = \hat{a}_m^\dagger|0\rangle$, where f_m describes the corresponding field mode which is a normalized solution to the Maxwell equations. In many optical systems, particularly those involving imaging or free-space propagation, it is natural to consider spatial modes where each mode function $f(r_\perp)$ depends only on the spatial coordinates transverse to the main propagation direction. An example of such modes is the Laguerre Gauss (LG) family of spatial functions.

After determining the family of spatial modes, the observable associated with measuring a photon in position r_\perp in an imaging plane is given by

$$\hat{N}(r_\perp) = \sum_{m,m'} \hat{a}_m^\dagger \hat{a}_{m'} f_m^*(r_\perp) f_{m'}(r_\perp) \quad (1)$$

Where $\{f_m(r_\perp)\}_{m=1}^d$ are the spatial modes in the Hilbert space $\mathcal{H}_{\text{spatial}}^{(d)}$ of dimension d . For a state ρ in this space, the probability of measuring a photon at position $r_\perp = (x, y)$ is given by:

$$P(r_\perp) = Tr \left(\rho \hat{N}(r_\perp) \right) = Tr(\rho |r_\perp; d\rangle\langle r_\perp; d|) \quad (2)$$

where $|r_\perp; d\rangle = \sum_{l=1}^d f_l^*(r_\perp) |f_l\rangle$ is the superposition of spatial states at pixel r_\perp , which we denote as the pixel state. Given a pixel with area \mathcal{S} , the probability of detecting a photon is $\int_{\mathcal{S}} P(r_\perp) dr_\perp = Tr(\rho \int_{\mathcal{S}} |r_\perp; d\rangle\langle r_\perp; d| dr_\perp)$. For simplicity and readability, we assume a sufficiently small \mathcal{S} such that $\int_{\mathcal{S}} P(r_\perp) dr_\perp \approx P(r_\perp)$. However, this assumption is not essential, and the following theory remains valid without it.

An intensity image measured at n pixel positions $\{r_i\}_{i=1}^n$ with N photons is formed by N independent draws from the discrete distribution $P(r_i)$. This type of measurement corresponds

to a Positive Operator-Valued Measure (POVM) [33]. Defining the positive semidefinite operators $\Pi_i = |r_\perp; d\rangle\langle r_\perp; d|$, and assuming the image area covers the support of all modes such that $\sum_{i=1}^n P(r_i) = 1$, we find that $\sum_{i=1}^n \Pi_i = I$, satisfying the conditions for a POVM.

To allow reconstruction, the POVM must be informationally complete (IC), meaning that no two different density matrices will result in the same spatial distribution [34]. Intuitively, if two states are different, there exists some physical observable that can distinguish between them. An IC POVM must be able to represent every such observable. Mathematically, this translates to the set $\{\Pi_i\}_{i=1}^n$ spanning the space of Hermitian operators acting on $\mathcal{H}_{\text{spatial}}^{(d)}$ [35–37]. Weaker conditions can be found if some prior information on the state exists, such as a bound on its rank [37,38].

The need for a coupler: intensity measurements are not IC

If the spatial modes do not satisfy the IC condition, direct measurement alone is insufficient to recover the state, as the same intensity image can result from different states. A typical example for two different modes that do not satisfy the IC condition hence cannot be distinguished by a direct intensity measurement alone are paraxial OAM states, given by:

$$LG_{lp} \propto \exp\left[-\frac{r^2}{w^2(z)}\right] L_p^{|l|} \left(\frac{2r^2}{w^2(z)}\right) \exp[il\phi] \quad (3)$$

where $w(z) = w(0)\sqrt{(z^2 + z_R^2)/z_R^2}$ with $w(0)$ the beam waist, z_R the Rayleigh range, and $L_p^{|l|}$ is an associated Laguerre polynomial [39]. l is the azimuthal index determining the quanta of OAM of the photon, and p is the number of radial nodes in the intensity of the mode. Equation (3) shows that the sign of the azimuthal index of an LG mode only affects its phase, meaning that two OAM modes with opposite momentum have the same intensity profile and so the POVM they define does not hold the condition for IC (see Fig. 1(a)). In these cases, one needs to expand the measurement space. For instance, in [40] the reconstruction of spatially structured light required a second intensity measurement, applying a unitary transformation \mathcal{U} on the state beforehand. While this doubled the number of measurements, it formed an IC set allowing full recovery.

When considering a hyperentangled state, the IC condition of the spatial modes is not enough to guarantee that two states will result in different measurements, simply because some DOFs are not visible to cameras. Consider a state ρ prepared in the composite Hilbert space $\mathcal{H}_{\text{spatial}}^d \otimes \mathcal{H}_{\text{non-spatial}}^m$, where d represents the number of spatial modes and m corresponds to the modes of a non-spatial DOF. Examples of such ubiquitous DOFs are frequency,

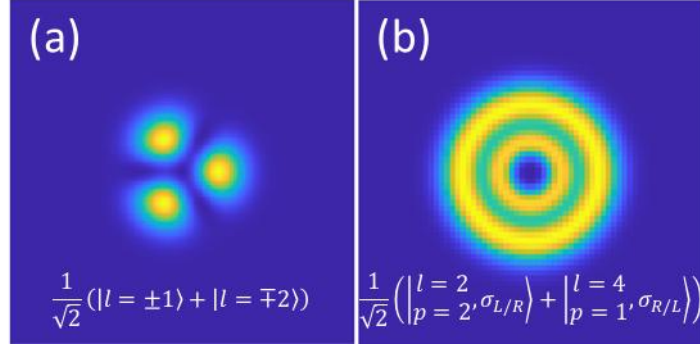


Fig. 1. Examples of fail cases for distinguishing states from intensity measurements. (a) Intensity ambiguity when the spatial modes do not hold the condition for IC. The OAM states $|l = \pm 1\rangle$ and $|l = \mp 2\rangle$ have the same intensity profile resulting in the two states $\frac{1}{\sqrt{2}}(|l = \pm 1\rangle + |l = \mp 2\rangle)$ producing the same measurement. (b) The two hyperentangled states only differ in their spin DOF resulting in the same intensity measurement even though the spatial modes $\{l = 2, p = 2\}, \{l = 4, p = 1\}$ hold the condition for IC separately.

polarization, time bins etc. Importantly, $\mathcal{H}_{\text{non-spatial}}^m$ can be a tensor product of multiple non-spatial DOFs spaces. As we show below, using a coupler that couples spatial to non-spatial DOFs, our method can also recover the latter, thereby recovering more than two DOFs in a single measurement. Since the non-spatial DOFs are invisible to the camera, the probability of a photon incidence on a pixel is determined only by the partial trace of ρ over $\mathcal{H}_{\text{non-spatial}}^m$.

$$P(r_\perp) = \text{Tr}(\text{Tr}_m(\rho) |r_\perp; d\rangle\langle r_\perp; d|) \quad (4)$$

Thus, even if the spatial modes do form an IC POVM, only $\text{Tr}_m(\rho)$ can be determined using a direct intensity measurement. To address this problem, we note that the Hilbert space of photonic spatial modes is in fact infinite. We can consider ρ as a state in a larger Hilbert space $\mathcal{H}_{\text{spatial}}^D \otimes \mathcal{H}_{\text{non-spatial}}^m$, where $D - d > 0$ additional spatial modes are included, and their corresponding entries in ρ are zero i.e., they are ancilla modes. While the natural spatial structure of light offers us these ancilla modes, to be of use for reconstruction - one needs to be able to transfer the state information (especially the non-spatial modes) onto these ancillas.

Coupler lifting and reconstruction formulation

To recover the missing information from the non-spatial DOFs and encode it onto the ancilla modes, we propose propagating the state through a coupling system \mathcal{U} . This results in a modified version of Eq. (4)

$$P(r_\perp) = \text{Tr}(\text{Tr}_m(\mathcal{U}\rho\mathcal{U}^\dagger) |r_\perp; D\rangle\langle r_\perp; D|) \quad (5)$$

Since we aim to recover a state from a $d \times m$ dimensional space by encoding it into a D -dimensional state, a necessary condition for a successful recovery is that:

$$D \geq dm \quad (6)$$

Similar to the case of measuring without a coupler, the coupled measurement can be presented as a POVM measurement defined by (see Appendix A):

$$\Pi_i(\mathcal{U}) = \mathcal{U}^\dagger (|r_\perp; D\rangle\langle r_\perp; D| \otimes I_m) \mathcal{U} \quad (7)$$

where I_m is the identity operator in the non-spatial DOF space. The probability of a photon incidence on pixel at position r_i is then given by:

$$P(r_i) = \text{Tr}(\rho \Pi_i(\mathcal{U})) \quad (8)$$

As with the spatial case, the POVM $\{\Pi_i(\mathcal{U})\}_{i=1}^n$ allows for a complete recovery if and only if it meets the condition for an IC POVM, i.e., spans the space of Hermitian operators of dimension $dm \times dm$. Choosing to represent the measurement process as a POVM (Eq. (7)), instead of the representation in Eq. (5), is not only mathematically compact and elegant but also can significantly lower the computational cost of the reconstruction process by allowing to precompute the operators involved (Appendix B)

Our reconstruction process (Fig. 2) begins by acquiring an intensity image $\{I(r_i)\}_{i=1}^n$ of the state after it propagates through the (coupling) system, with N photons detected. Using this image, we estimate the photon spatial distribution with $P(r_i) = I(r_i)/N$. Note that, even if in practice the number of photons is not known precisely, one can approximate it by normalizing the total signal obtained on the camera over the entire integration time, yielding a normalized intensity representing the probability. To reconstruct a density matrix, ρ , that best describes the measurements of the intensity image, we formalize the recovery as a constrained least squares problem, resulting in a quadratic and convex optimization problem given in the following form:

$$\min_{\rho} \sum_{i=1}^n \left| \text{Tr}(\rho \Pi_i(\mathcal{U})) - \frac{I(r_i)}{N} \right|^2 \quad (9)$$

$$\text{s.t. } \rho = \rho^\dagger, \quad \rho \geq 0, \quad \text{Tr}(\rho) = 1$$

This formulation is standard and can be solved by a variety of methods and approaches. In our work we used CVX [41,42], a package for specifying and solving convex programs. The

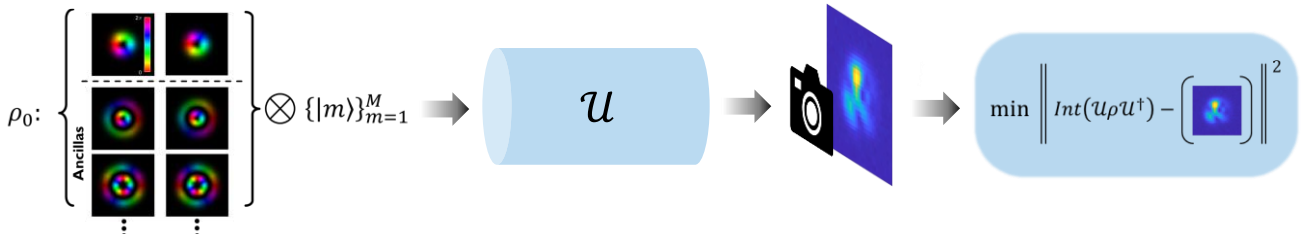


Fig. 2. Reconstruction scheme. A state propagates through a coupling system mixing its information onto the spatial modes and afterwards it is imaged. The state is recovered by solving the optimization problem minimizing the L2-error between the measured and estimated intensity image.

specific details of our coupling system are described in the following sections along with important computational and noise considerations.

Results

In the following sections, we present the reconstruction performance of our method using simulated data. We evaluate the framework across different coupling systems and photonic DOFs to demonstrate its generalizability. We begin with the simplest case: recovering the spatial DOF with an ideal random coupler. Next, we extend the methodology to joint spatial and polarization DOFs (states entangled in their spin and OAM) using a physically realizable coupler based on a multi-mode fiber (MMF). For completeness, we also show in the Appendix how the fiber medium can be extended, via cross-phase modulation, to couple and recover the frequency DOF of light. Finally, we extend our analysis to the multiphoton regime, which is essential for many applications, and presents unique challenges.

Random Coupler

As a first step, we evaluate our method under general conditions using a simulated random coupler that is sampled uniformly from the unitary group [28]. This ensures that the information encoded in the quantum state is well-distributed across the output spatial modes, resulting in

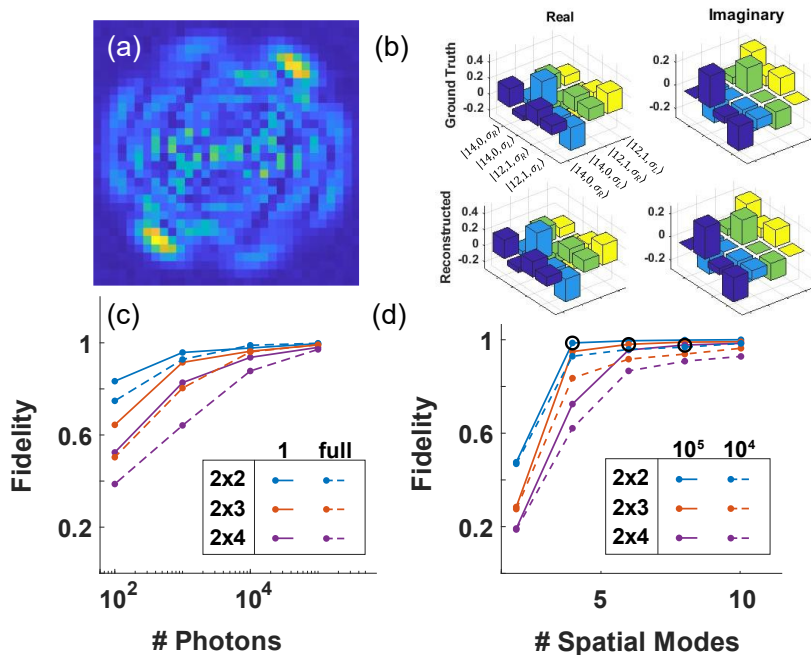


Fig. 3. (a) Intensity measurement of a state of 2 LG modes and 2 non-spatial modes of rank-1 using an ideal coupler with 6 ancillas. The total system has 16 modes $\{|l, p, \sigma_{R/L}\}\}$ with a constant total order $2p + |l| = 14$ (b) Reconstruction of the state using an ideal coupler with fidelity 0.99. Top plot shows the ground truth while the bottom shows the reconstructed density matrix. (c) Mean fidelity of reconstructed density matrices versus number of detected photons. Results are plotted for rank 1 (solid) and full rank (dashed) states with 2 LG modes and 2,3, and 4 non-spatial DOFs. The coupler used with 10 ancilla modes. (d) Mean fidelity versus number of total spatial modes (2 + ancillas) for the same states as in (c). Solid (dashed) lines correspond to 10^5 (10^4) detected photons. Circled points correspond to the equality in Eq. (5), marking the threshold for reconstruction.

POVM elements that are as uncorrelated as possible. We choose to test our method with LG modes with a constant total order $2p + |l|$, which are IC [40]. We note however that choosing an IC set of spatial modes is not strictly necessary. When the modes are not IC, the coupler will simply require more ancilla modes for full reconstruction.

To illustrate the reconstruction process, we first consider a pure random state of 2 spatial modes and 2 non-spatial modes. A random coupler of 6 ancilla modes is used, mixing the state information onto a space of total 8 spatial modes. The spatial distribution captured after the random coupler (shown in Fig. 3(a)) serves as the input to the optimization algorithm. The reconstructed density matrix matches the target state with a fidelity of more than 0.99.

We analyze the method's performance across varying state dimensions and ranks, and validate its robustness to noise and finite photon counts. In our simulation, we consider a quantum state ρ_0 of dimension $d \times m$, of d spatial and m non-spatial modes, of pure (rank 1) or full-rank $d \times m$. The state is passed through the coupler that mixes its information onto D spatial modes. A $N \times N$ intensity image of n photons is then obtained by sampling from the spatial distribution following Eq. (8). Additive white Gaussian noise is then added to simulate realistic noisy conditions. Fig. 3(a) shows such a measurement with $N = 32$, $n = 10^5$, and 30 dB SNR. These simulated measurements are used as input to our reconstruction algorithm, which solves Eq. (9) to estimate the state ρ_{rec} . The fidelity between the original and

reconstructed states is computed as $F(\rho_0, \rho_{rec}) = \left(\text{Tr} \sqrt{\rho_0^{\frac{1}{2}} \rho_{rec} \rho_0^{\frac{1}{2}}} \right)^2$. The average fidelity over

50 random state initializations is plotted in Fig. 2(c) as a function of the number of photons with a constant number of spatial modes fixed to 10 and as a function of the number of spatial modes in Fig. 3(d) for different state dimensions. We observe that for 10^5 photons, all states are recovered with a mean fidelity over 0.97, regardless of dimension and rank, indicating that this photon budget allows for good estimation. This is further illustrated in Fig. 3(d), where the fidelity improves as the number of ancillas increases when the photon count is low (dotted lines). This supports the intuition that, given a good coupler, increasing the number of ancillas increases measurement redundancy, making the estimation more robust to errors. The solid curves in Fig. 3(d), corresponding to the high photon count, present a knee at the point satisfying condition (5) after which the fidelity plateaus. This is expected as this necessary condition becomes sufficient when the spatial modes form an IC family and the coupler mixing properties are sufficiently good.

OAM-Spin States

Building on these results for spatial DOFs with an ideal coupler, we next consider states entangled across both spatial and polarization DOFs (OAM-spin), using a physically realizable coupling system based on a multi-mode fiber. One example of single-photon hyperentanglement is the entanglement between the Spin and OAM DOFs of a single photon, which was recently shown experimentally using metamaterials [26] to encode two qubits on a single photon, and has a potential for increasing channel capacity in quantum communication [16]. The Hilbert space of OAM-carrying states is expressed in the orthonormal base of LG modes given in Eq. (3), where the azimuthal index l determines the quanta of OAM of the photon.

We want to recover a state $\rho \in \mathcal{H}_{OAM}^d \otimes \mathcal{H}_{spin}^2$ of a single photon entangled between d OAM modes and its spin DOF. For our POVM from (7) to be IC, we need a coupling system \mathcal{U} that “mixes well enough” different OAM-spin states. For this, we suggest to harness the intrinsic spatial- and polarization- mode coupling in a multimode fiber. The classically acquired transmission matrix (TM) of a multimode fiber has been shown to allow control of quantum light inside the fiber [43,44]. Thus, to model our forward process in (7) we can use the TM as our unitary \mathcal{U} . We demonstrate our reconstruction method using the experimentally measured TM in [45]. The TM characterizes a 2m graded-index fiber with a core diameter of $62.5\mu m$ at wavelength of $1525nm$ with 420 modes.

Looking at the reconstruction results in Fig. 4, we see that, for a low photon count (a low accuracy of the estimated photon distribution), successful reconstruction depends on the rank of the state. On the other hand, for high photon counts the results are only weakly dependent on whether the state is pure or mixed, suggesting that the coupler is close to ideal. Indeed, the

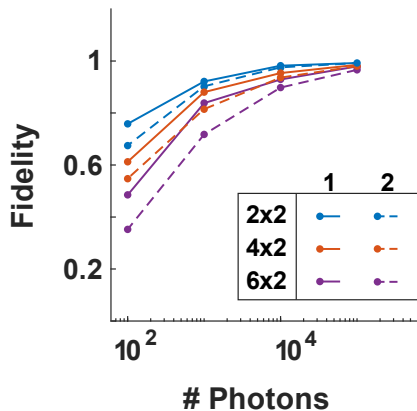


Fig. 4. OAM-Spin states reconstruction using a multi-mode optical fiber acting as a coupler between spatial modes. The figure shows the fidelity as a function of the number of photons for different state dimensions and rank.

condition for an informationally complete POVM is met for the TM and for the reconstructed dimensions of the states.

Having demonstrated reconstruction of OAM-spin states with a multi-mode fiber coupler, we note that our framework can be extended to frequency DOFs as well. A detailed discussion and numerical simulations, including spatio-spectral coupling via Kerr-induced cross-phase modulation, are provided in Appendix C. Importantly, this implies that this approach could be extended to recover states entangled across all three DOFs - spatial, spectral, and spin.

Multiphoton Hyperentangled States

Finally, we extend our analysis to the multiphoton regime, examining the limitations and requirements for tomography of hyperentangled states with a single measurement setup. For clarity, we examine a bi-photon state, of photons A and B, in the cross-product space $\mathcal{H}_A \otimes \mathcal{H}_B$ of two identical spaces of d spatial and m non-spatial modes in each. What information is obtained by naively using the single photon scheme on this state? Passing both photons through the coupling system, the intensity at each pixel no longer corresponds to a standard POVM. This is because the measurement cannot distinguish whether a single-photon is incident or two photons are incident on the same pixel. Respectively, the probabilities of these events are:

$$P_1 = \text{Tr} \left(\frac{1}{2} (\Pi_i(\mathcal{U}) \otimes I + I \otimes \Pi_i(\mathcal{U})) \rho \right) - \text{Tr}(\Pi_i(\mathcal{U}) \otimes \Pi_i(\mathcal{U}) \rho) \quad (10)$$

$$P_2 = \text{Tr}(\Pi_i(\mathcal{U}) \otimes \Pi_i(\mathcal{U}) \rho) \quad (11)$$

where i is the pixel measured, $\Pi_i(\mathcal{U})$ is given in Eq. (7), and \mathcal{U} is a unitary operation acting on a single-photon space. The left term in Eq. (10) corresponds to the POVM of observing any incident, one or two photons on pixel i . Eq. (11) corresponds to the POVM of both photons incident on the same pixel. Integrating over many events, an intensity image is formed, and the two probabilities determine the probability of the measurement by:

$$P(I_i = k) = \sum_{j=0}^{\lfloor k/2 \rfloor} P_1^{k-2j} P_2^j \quad (12)$$

Where k is the photon count number at pixel i . Even if P_1, P_2 could be inferred from Eq. (12), and the single-photon POVM in Eq. (7) was IC, dimensionality analysis shows the resulting measurement is not IC for this bi-photon space. Intuitively, this is expected as the intensity measurement should result in superposition of the intensity distribution for each photon, superimposed on top of one another at the detector and it is blind to their correlations. Therefore,

to recover the full multiphoton state, the measurement will require the interaction between the photons to be sensitive to the multiphoton correlations in a single measurement.

This insight leads to the following implications. Mathematically, the choice between the individual photons can be thought of as another DOF. As such, we can design a coupling system that will inter-operate on the two photon subspaces, meaning that \mathcal{U} is no-longer a product of two single-photon operators. Based on our previous analysis of the single-photon case, a system that mixes the information between different DOFs and different photon subspaces will result in an IC measurement given by Eq. (7), using only an intensity measurement. However, this dictates that the system will require a two-photon nonlinearity or a two-photon entangling property, which can be challenging especially at low intensities of single photons.

To circumvent this, we can relax the requirement of using a single intensity measurement. Notice that given a single-photon IC POVM of n operators, $\Pi_i(\mathcal{U})$, the bi-photon POVM, $\Pi_i(\mathcal{U}) \otimes \Pi_j(\mathcal{U})$, of n^2 operators is IC. This corresponds to a spatial coincidence measurement [46–48] between the two photons after propagating them through the coupling system. Although coincidence measurements are experimentally more demanding, this theoretically allows for full tomography of multiphoton spatially hyperentangled states in a single setup, which has thus far never been suggested.

Extending this to N -photon state requires an N -fold coincidence measurement. While this scales exponentially with the number of photons, we note that this is a general challenge of multiphoton tomography and not unique to our method, and existing mitigation approaches can be applied [27].

Notably, this framework extends beyond photonics to other quantum processing platforms. For instance, work by Stricker et al. [29] demonstrated a single-setting QST on an ion trap quantum processor. By projecting each qubit into a four-level system, utilizing high-level energy levels as ancillas, they performed QST via a single coincidence measurement. Our framework captures this by choosing a qubit system ($d = 2$) with no additional DOFs ($m = 1$), a coupler into a $D = 4$ space, and utilizing a coincidence measurement as the measurement modality. This demonstrates that this framework, although intended for photonic systems, is more general and applicable to other quantum processing platforms that offer access to high dimensional states allowing for a minimal tomography scheme.

Conclusions

We introduced a general framework for the tomography of general single-photon states, entangled between multiple photonic DOFs, using a single intensity measurement. Our framework hinges on the ability to construct a coupler that can mix between arbitrary spatial DOFs and non-spatial DOFs, enabling full encoding of the state's information into the spatial intensity pattern. This method eliminates the need for multiple measurement configurations, reducing experimental complexity and lowering errors from setup reconfiguration, and allowing for a faster reconstruction time. We demonstrated numerically how states entangled between their OAM and spin, and between their OAM and frequency, can be reconstructed using a coupler based on a MMF and the XPM effect. Importantly, we showed how these reconstruction schemes can be easily realized using the MMF classical TM and the introduced spatio-spectral TM allowing for a low computational cost. We also presented an extension of this method for reconstructing multiphoton hyperentangled states by replacing the single intensity with a single coincidence measurement. While this is more experimentally demanding, it enables full tomography of multiphoton states in a single measurement setup.

We envision that this general approach can be applied across a wide range of platforms to enable the reconstruction of single-photon hyperentangled states and beyond. In particular, integrated photonic devices are well-suited to this framework, offering a path toward compact, scalable, and fully integrated solutions for quantum state characterization. We are currently working towards an experimental demonstration that showcase our method in the lab. Future directions include optimizing the design of couplers and measurement schemes, analyzing robustness to noise, exploring spatial and time-bins coupling, and demonstrating the framework extension to multi-photon states.

Appendix A: Proof of Equation (7)

We prove that Eq. (8) is equivalent to Eq. (4). Substituting (7) into (8) and using the cyclic property of the trace, we find that

$$Tr(\rho \Pi_i(\mathcal{U})) = Tr(\mathcal{U} \rho \mathcal{U}^\dagger (|r_\perp; D\rangle \langle r_\perp; D| \otimes I_m)) \quad (A1)$$

For any operator $\mathcal{O} \in \mathcal{H}_A$ and a system $\sigma \in \mathcal{H}_A \otimes \mathcal{H}_B$, the partial trace is exactly defined such that operating with \mathcal{O} on $Tr_B(\sigma)$ is equivalent to operating on the entire system with $\mathcal{O} \otimes I_B$. Using $\mathcal{O} = |r_\perp; D\rangle \langle r_\perp; D|$ and $\sigma = \mathcal{U} \rho \mathcal{U}^\dagger$ gives us Eq. (4).

Appendix B: Numerical considerations of POVM description

Equation (4) gives a natural and simple description of the measurement process. A state $\rho \in \mathcal{H}_{\text{spatial}}^d \otimes \mathcal{H}_{\text{non-spatial}}^m$ propagates through the coupler $\mathcal{U} \in \mathbb{C}^{Dm \times dm}$, resulting in the output state $\mathcal{U}\rho\mathcal{U}^\dagger \in \mathcal{H}_{\text{spatial}}^D \otimes \mathcal{H}_{\text{non-spatial}}^m$. This state is then measured by a camera which is blind to the non-spatial DOF, hence the measurement is performed only on the spatial subsystem, mathematically described by the partial trace on the state. However, when solving the optimization problem (9), this description necessitates calculation of $\rho \rightarrow \text{Tr}_m(\mathcal{U}\rho\mathcal{U}^\dagger)$ for every iteration, which is inefficient in time and memory complexity. Describing the measurement as a POVM (Eq. (8)) allows to calculate the POVM operators in Eq. (7) in advance, and during the optimization one only needs to perform the matrix multiplication between matrices of identical dimension $dm \times dm$.

Additionally, due to the unique structure of the POVM matrices in Eq. (7), also their calculation can be performed efficiently in terms of the required memory, which is necessary for large coupling matrices. Given three matrices, $A, C^T \in \mathbb{C}^{s \times dm}, B \in \mathbb{C}^{d \times d}$, where A is built by stacking d blocks of dimension $s \times m$, and similarly C is the concatenation of d blocks of dimension $m \times s$. We mark these blocks $A_i^{s \times m}$ and $C_i^{m \times s}$. It can be shown that

$$A \cdot (B \otimes I_m) \cdot C = \sum_{i,j=1}^d B_{ij} \cdot A_i^{s \times m} C_j^{m \times s} \quad (\text{B2})$$

Where I_m is the $m \times m$ identity matrix and B_{ij} is the ij entry of B .

Appendix C: OAM-Frequency bins states

Beyond spatial and spin DOFs, frequency-bin encoding provides a highly scalable resource for photonic quantum information processing. In this appendix, we demonstrate how our framework can be adapted to frequency DOFs by leveraging nonlinear interactions, specifically cross-phase modulation, in multi-mode fibers.

The operational Hilbert space we consider consists of m frequency bins - electromagnetic modes of identical spectral shape that are evenly spaced in frequency. While the previously suggested coupling system, based on a MMF, demonstrates effective spatial mode coupling, its linear and time-invariant nature prevents coupling between frequency-bins and spatial modes. To overcome this limitation, we suggest leveraging the Kerr nonlinearity – specifically, the cross-phase modulation (XPM) effect between a strong pump and the single-photon field [49,50]. Modulating the pump’s envelope at a frequency matching the bin spacing creates

a modulation in the refractive index in the fiber. This facilitates coupling between frequency-bins, analogous to the mechanism of electro-optic phase modulators used in frequency-bin photonic quantum information [51].

The interaction between the pump and single-photon fields inside the MMF is governed by a set of coupled nonlinear Schrodinger-like equations, which account for the frequency difference between the pump and photon. However, for weak fields - such as a single-photon state, and a non-depleted pump, these equations become effectively linear for the single-photon fields. This is a crucial observation for the experimental realization of our system, as it implies that the system's operation can be fully characterized by a spatio-spectral TM, analogous to the familiar TM used in our reconstruction of OAM-spin states.

To construct the spatio-spectral TM, we determine the system's response to a set of orthogonal input signals spanning all combinations of spatial and frequency modes. By projecting the output signals onto this same orthogonal set, we obtain the columns of the TM. To account for the potential temporal distortions at the output, one can also incorporate a family of orthogonal temporal modes, such as Hermite-Gaussian functions [52], increasing the orthogonal set.

We demonstrate our method numerically [53], simulating a 0.5 meter long, graded index few-modes fiber. The fiber is pumped with a 1nsec width, 0.5pJ pulse at 1800nm , where supports 3 spatial modes. The pump's envelope is modulated at 1THz , matching the spacing between adjacent frequency bins. At the single-photon wavelength of 900nm , the fiber supports 10 spatial modes. These wavelengths are chosen both to reduce computational time (by reducing the number of modes at the pump's wavelength) and to ensure similar group velocities between the pump and single-photon, thereby enhancing interaction efficiency. While the pump and photon experience chromatic dispersion with opposite signs, this effect is negligible due to the short fiber length.

For computational feasibility, we restrict our reconstruction to states prepared with 3 frequency-bins centered around 900nm and spaced 1THz apart. The spatio-spectral TM of the system is constructed by propagating each of these frequency bins across all 10 spatial modes. Due to coupling between adjacent bins, the output pulses span 5 frequency-bins and are also projected onto the first 3 Hermite-Gaussian modes. This results in a 150×30 TM. As in the reconstruction of OAM-spin states, the unitary \mathcal{U} is obtained by transforming the TM into the OAM basis.

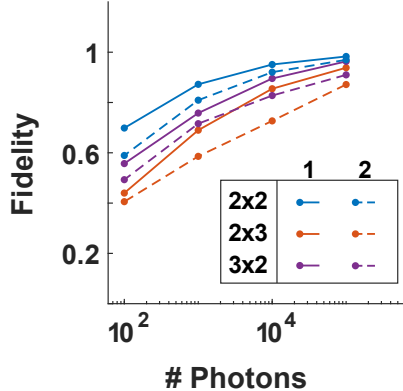


Fig. 5. Reconstruction results of OAM-Frequency states plotted for different dimensions and ranks of the initial state.

The reconstruction results in Fig. 5 display a behavior similar to our previous cases. Perhaps not surprisingly, it can be seen that increasing the number of non-spatial DOF, invisible to the camera, results in worse results than for states with the same dimension but with increased spatial modes. Another observation is that contrary to our previous examples, although the coupler does form an informationally complete POVM, for a photon count of 10^5 the result is dependent on the state's rank. This indicates that this coupler does not provide enough redundancy as the previous couplers. This can be improved by increasing the number of ancilla modes by using a fiber with additional supported modes. We note that our choice of a few-mode fiber with 10 modes is only a restriction of the computation power needed to simulate the system. In a real lab setup, the spectral TM can be obtained for a MMF, using a greater number of ancillas and improving the mixing properties of the coupler.

MMFs can also support strong spatial-polarization coupling, as experimentally observed [45]. Although outside the scope of our simulation, this implies that by utilizing a MMF as a coupler, it is possible to recover quantum states entangled across all three DOFs, spatial, spectral and spin.

Disclosure. The authors declare no conflicts of interest.

Data availability. All data generated and analyzed during this study are available from the corresponding author on reasonable request.

References

1. I. A. Walmsley, "Quantum optics: Science and technology in a new light," *Science* **348**, 525–530 (2015).
2. J. Wang, F. Sciarrino, A. Laing, et al., "Integrated photonic quantum technologies," *Nat. Photonics* **14**, 273–284 (2020).
3. N. Gisin and R. Thew, "Quantum communication," *Nat. Photonics* **1**, 165–171 (2007).
4. A. Aspuru-Guzik and P. Walther, "Photonic quantum simulators," *Nat. Phys.* **8**, 285–291 (2012).
5. J. L. O'Brien, "Optical quantum computing," *Science* **318**, 1567–1570 (2007).

6. E. Knill, R. Laflamme, and G. J. Milburn, "A scheme for efficient quantum computation with linear optics," *Nat.* **409**, 46–52 (2001).
7. G. J. Milburn, "Photons as qubits," *Phys. Scr.* **2009**, 014003 (2009).
8. P. Imany, J. A. Jaramillo-Villegas, M. S. Alshaykh, et al., "High-dimensional optical quantum logic in large operational spaces," *Npj Quantum Inf.* **5**, 59 (2019).
9. C. Reimer, M. Kues, P. Roztocki, et al., "Generation of multiphoton entangled quantum states by means of integrated frequency combs," *Science* **351**, 1176–1180 (2016).
10. J. Leach, B. Jack, J. Romero, et al., "Quantum Correlations in Optical Angle–Orbital Angular Momentum Variables," *Science* **329**, 662–665 (2010).
11. C. He, Y. Shen, and A. Forbes, "Towards higher-dimensional structured light," *Light Sci. Appl.* **11**, 205 (2022).
12. M. Mirhosseini, O. S. Magaña-Loaiza, M. N. O'Sullivan, et al., "High-dimensional quantum cryptography with twisted light," *New J. Phys.* **17**, 033033 (2015).
13. A. Sit, F. Bouchard, R. Fickler, et al., "High-dimensional intracity quantum cryptography with structured photons," *Optica* **4**, 1006–1010 (2017).
14. P. G. Kwiat, "Hyper-entangled states," *J. Mod. Opt.* **44**, 2173–2184 (1997).
15. J. T. Barreiro, T. C. Wei, and P. G. Kwiat, "Beating the channel capacity limit for linear photonic superdense coding," *Nat. Phys.* **4**, 282–286 (2008).
16. L. Nemirovsky-Levy, U. Pereg, and M. Segev, "Increasing quantum communication rates using hyperentangled photonic states," *Opt. Quantum* **2**, 165–172 (2024).
17. Y. B. Sheng, L. Zhou, and G. L. Long, "One-step quantum secure direct communication," *Sci. Bull.* **67**, 367–374 (2022).
18. J.-H. Kim, Y. Kim, D.-G. Im, et al., "Noise-resistant quantum communications using hyperentanglement," *Opt.* **8**, 1524–1531 (2021).
19. P. G. Kwiat and H. Weinfurter, "Embedded Bell-state analysis," *Phys. Rev. A* **58**, R2623 (1998).
20. M. Fiorentino and F. N. C. Wong, "Deterministic controlled-NOT gate for single-photon two-qubit quantum logic," *Phys. Rev. Lett.* **93**, 070502 (2004).
21. K. H. Kagalwala, G. Di Giuseppe, A. F. Abouraddy, et al., "Single-photon three-qubit quantum logic using spatial light modulators," *Nat. Commun.* **8**, 1–11 (2017).
22. D. F. V. James, P. G. Kwiat, W. J. Munro, et al., "Measurement of qubits," *Phys. Rev. A* **64**, 052312 (2001).
23. N. K. Langford, R. B. Dalton, M. D. Harvey, et al., "Measuring entangled qutrits and their use for quantum bit commitment," *Phys. Rev. Lett.* **93**, 053601 (2004).
24. B. Jack, J. Leach, H. Ritsch, et al., "Precise quantum tomography of photon pairs with entangled orbital angular momentum," *New J. Phys.* **11**, 103024 (2009).
25. M. Agnew, J. Leach, M. McLaren, et al., "Tomography of the quantum state of photons entangled in high dimensions," *Phys. Rev. - At. Mol. Opt. Phys.* **84**, 062101 (2011).
26. T. Stav, A. Faerman, E. Maguid, et al., "Quantum entanglement of the spin and orbital angular momentum of photons using metamaterials," *Science* **361**, 1101–1104 (2018).
27. D. Oren, M. Mutzafi, Y. C. Eldar, et al., "Sparsity-based recovery of three-photon quantum states from two-fold correlations," *Opt.* **3**, 226–232 (2016).
28. D. Oren, M. Mutzafi, Y. C. Eldar, et al., "Quantum state tomography with a single measurement setup," *Opt.* **4**, 993–999 (2017).
29. R. Stricker, M. Meth, L. Postler, et al., "Experimental Single-Setting Quantum State Tomography," *PRX Quantum* **3**, 040310 (2022).
30. Y. Li, S.-Y. Huang, M. Wang, et al., "Two-Measurement Tomography of High-Dimensional Orbital Angular Momentum Entanglement," *Phys. Rev. Lett.* **130**, (2023).
31. D. Zia, N. Dehghan, F. Sciarrino, et al., "Interferometric imaging of amplitude and phase of spatial biphoton states," *Nat. Photonics* **17**, 1009–1016 (2023).
32. C. Fabre and N. Treps, "Modes and states in quantum optics," *Rev. Mod. Phys.* **92**, 035005 (2020).
33. H. E. Brandt, "Positive operator valued measure in quantum information processing," *Am. J. Phys.* **67**, 434–439 (1999).
34. E. Prugovečki, "Information-theoretical aspects of quantum measurement," *Int. J. Theor. Phys.* **16**, 321–331 (1977).
35. G. M. D'Ariano, P. Perinotti, and M. F. Sacchi, "Informationally complete measurements and group representation," *J. Opt. B Quantum Semiclassical Opt.* **6**, S487 (2004).
36. A. J. Scott, "Tight informationally complete quantum measurements," *J. Phys. A. Math. Gen.* **39**, 13507 (2006).

37. C. Carmeli, T. Heinosaari, J. Schultz, et al., "Tasks and premises in quantum state determination," *J. Phys. A. Math. Theor.* **47**, 075302 (2014).
38. C. H. Baldwin, I. H. Deutsch, and A. Kalev, "Strictly-complete measurements for bounded-rank quantum-state tomography," *Phys. Rev. A* **93**, 052105 (2016).
39. A. M. Yao and M. J. Padgett, "Orbital angular momentum: origins, behavior and applications," *Adv. Opt. Photonics* **3**, 161–204 (2011).
40. M. G. de Oliveira, A. L. S. Santos Junior, P. M. R. Lima, et al., "Informationally complete orbital-angular-momentum tomography with intensity measurements," *Phys. Rev. Appl.* **24**, 024031 (2025).
41. Inc. CVX Research, "CVX: Matlab Software for Disciplined Convex Programming, version 2.0," (2012).
42. M. Grant and S. Boyd, "Graph implementations for nonsmooth convex programs," in *Recent Advances in Learning and Control*, V. Blondel, S. Boyd, and H. Kimura, eds., *Lecture Notes in Control and Information Sciences* (Springer, 2008), Vol. 371.
43. J. Carpenter, C. Xiong, M. J. Collins, J. Li, T. F. Krauss, B. J. Eggleton, A. S. Clark, and J. Schröder, "Mode multiplexed single-photon and classical channels in a few-mode fiber," *Opt. Express* **21**, 28794–28800 (2013).
44. S. Leedumrongwatthanakun, L. Innocenti, H. Defienne, et al. "Programmable linear quantum networks with a multimode fibre," *Nat. Photonics* **14**, 139–142 (2020).
45. B. J. Eggleton, J. Carpenter, and J. Schröder, "Complete spatiotemporal characterization and optical transfer matrix inversion of a 420 mode fiber," *Opt. Lett.* **41**, 5580–5583 (2016).
46. T. B. Pittman, Y. H. Shih, D. V. Strekalov, et al., "Optical imaging by means of two-photon quantum entanglement," *Phys. Rev. A* **52**, R3429 (1995).
47. H. Defienne, M. Reichert, and J. W. Fleischer, "General Model of Photon-Pair Detection with an Image Sensor," *Phys. Rev. Lett.* **120**, 203604 (2018).
48. B. Ndagano, H. Defienne, A. Lyons, et al., "Imaging and certifying high-dimensional entanglement with a single-photon avalanche diode camera," *Npj Quantum Inf.* **6**, 94 (2020).
49. S. Matsuoka, N. Miyanaga, S. Amano, et al., "Frequency modulation controlled by cross-phase modulation in optical fiber," *Opt. Lett.* **22**, 25–27 (1997).
50. N. Matsuda, "Deterministic reshaping of single-photon spectra using cross-phase modulation," *Sci. Adv.* **2**, e1501223 (2016).
51. H.-H. Lu, M. Liscidini, A. L. Gaeta, et al., "Frequency-bin photonic quantum information," *Opt.* **10**, 1655–1671 (2023).
52. H. J. McGuinness, M. G. Raymer, C. J. McKinstrie, "Theory of quantum frequency translation of light in optical fiber: application to interference of two photons of different color," *Opt. Express* **19**, 17876–17907 (2011).
53. L. G. Wright, Z. M. Ziegler, P. M. Lushnikov, et al., "Multimode Nonlinear Fiber Optics: Massively Parallel Numerical Solver, Tutorial, and Outlook," *IEEE J. Sel. Top. Quantum Electron.* **24**, 1–16 (2018).